Reverse Osmosis Performance of Organosilica Membranes and Comparison with the Pervaporation and Gas Permeation Properties

Rong Xu, Jinhui Wang, Masakoto Kanezashi, Tomohisa Yoshioka, and Toshinori Tsuru
Dept. of Chemical Engineering, Hiroshima University, Higashi-Hiroshima 739-8527, Japan

DOI 10.1002/aic.13885
Published online September 28, 2012 in Wiley Online Library (wileyonlinelibrary.com).

Hybrid organosilica membranes were successfully prepared using bis(triethoxysilyl)ethane (BTESE) and applied to reverse osmosis (RO) desalination. The organosilica membrane calcined at 300°C almost completely rejected salts and neutral solutes with low-molecular-weight. Increasing the operating pressure led to an increase in water flux and salt rejection, while the flux and rejection decreased as salt concentration increased. The water permeation mechanism differed from the viscous flow mechanism. Observed activation energies for permeation were larger for membranes with a smaller pore size, and were considerably larger than the activation energy for water viscosity. The organosilica membranes exhibited exceptional hydrothermal stability in temperature cycles up to 90°C. The applicability of the generalized solution-diffusion (SD) model to RO and pervaporation (PV) desalination processes were examined, and the quantitative differences in water permeance were accurately predicted by the application of generalized transport equations. © 2012 American Institute of Chemical Engineers *AIChE J,* 59: 1298–1307, 2013
Keywords: reverse osmosis, membrane, organosilica, solution-diffusion model, pervaporation

Introduction

The provision of clean, fresh water for continuously growing populations is a long-term challenge facing the world today. Reverse osmosis (RO) is now the leading technology for the production of drinking water from seawater and brackish water, and its popularity is expected to increase in the near future.[1,2] A typical RO membrane is composed of a crosslinked aromatic polyamide thin film on the surface of a microporous polysulfone support via interfacial polymerization. These polyamide thin-film composite membranes dominate the current RO membrane market due to their high salt rejection (>99%) and high water permeability.[3] However, polyamide membranes are prone to biofouling, which severely diminishes filtration performance and shortens membrane lifetime.[4] The membrane biofouling could be reduced or even stopped if the oxidizing agents such as chlorine could be added to the feed. Unfortunately, polyamide membranes are quite sensitive to chlorine, because the amide linkage in the membranes is susceptible to chlorine attack.[5] Extensive efforts have, therefore, been devoted to developing new chlorine-resistant RO membranes, such as the recently exploited membranes based on crosslinked lyotropic liquid crystals and sulfonated block copolymers.[6–8] Moreover, operation of RO at high temperatures is desired in many industrial applications, such as the food and textile industries.[9,10] Unfortunately, the maximum operating temperature for most polyamide membranes is normally below 55°C.[10,11] Hence, a major objective in new RO membrane development is the combination of high permeability and selectivity, along with durability in harsh environments.

Inorganic membranes have superior thermal and chemical stability with great potential for application to water desalination. Recently, zeolite membranes such as MFI-type (silicalite and ZSM-5) zeolite, have been tried for RO desalination because of their well-defined sub-nanometer pore structures.[12–15] Zeolite membranes, however, typically require tedious synthesis procedures to form thin, defect-free film on porous substrates. Another promising candidate for RO desalination is amorphous microporous silica membranes with molecular sieving permeation characteristics. These sol–gel derived silica membranes with pore sizes that range from 2–5 Å have been successfully used for gas separation and pervaporation (PV) processes.[16–18] The main obstacle to the use of silica membranes for water purification is structural instability in the presence of water, due to hydrolysis of the siloxane bonds and rearrangement of the silanol groups, which eventually results in a loss of separation performance.[19] Some alternative approaches have been proposed to improve the hydrothermal stability of silica membranes, such as modification of silica matrix with metal oxides[20,21] or methyl (—CH_3) groups.[22,23]

More recently, some research groups have reported the utilization of organically bridged *bis*-silyl precursors for the fabrication of microporous organosilica membranes. The stability of the membranes has been greatly enhanced by incorporating organic linking groups between two silicon atoms.[24–28] Castricum et al.[24,25] developed microporous membranes derived

Correspondence concerning this article should be addressed to T. Tsuru at tsuru@hiroshima-u.a.c.jp.

from cocondensation of 1,2-bis(triethoxysilyl)ethane (BTESE) and methyltriethoxysilane (MTES) for the dehydration of 95 wt % n-butanol by PV. The results demonstrated that these organosilica membranes could withstand long-term operation of up to 2 years at 150°C. BTESE and bis(triethoxysilyl)methane (BTESM) membranes showed a high degree of acid stability in long-term measurements at a pH value of ≈2, and the membrane performance was reproducible for acidities that ranged from pH 2–8.[26] Our research group proposed a "spacer" technique to control silica networks, using an organically linked alkoxide for the development of a highly permeable hydrogen separation membrane with hydrothermal stability. Organosilica membranes derived from BTESE showed approximately one order of magnitude higher H_2 permeance, compared with previously reported tetraethoxysilane (TEOS)-derived silica membranes.[27,28]

A number of transport equations have been proposed for the transport mechanism. Gas permeation through porous membranes is governed by the viscous, Knudsen, surface diffusion, and molecular sieving mechanisms, depending on the pore size and the molecular size. One major transport theory for nonporous membranes is the solution-diffusion (SD) model in which the permeating molecules dissolve into a membrane, diffuse through it, and desorb from the other side. In liquid-phase separation, viscous flow is the accepted mechanism for the permeation of solvents in the range of MF to NF, while SD is the most widely accepted mechanism for transport in RO. The SD model was also applied to PV. Although the SD model has been used successfully for RO, PV and gas separation (GS), different types of SD equations have been used and the relationship among them is not clear. Several research groups have proposed a generalized SD model.[29–32] The more general equations provide a good description of transport behavior in all of these processes, and can be compared with each other. The generalized SD mode is valuable in predicting the flux in gas separation, PV and RO. However, only a limited number of articles have discussed the generalized SD model and examined its applicability.

Our most recent study examined the possibility of using BTESE-derived organosilica membranes to desalinate water by RO. These organosilica membranes exhibited exceptional chlorine tolerance and hydrothermal stability in our preliminary study, showing great promise as a new type of robust RO membrane materials.[33] For a better understanding of the permeation properties of this membrane, more detail is needed regarding the factors that affect membrane performance. In this article, we present the results of a series of studies including the effects of solute species, calcination temperatures and operational variables on membrane performances. Moreover, three different membrane processes, including RO, PV and gas permeation, were performed using the same organosilica membrane to study the transport properties in each process, and a quantitative comparison of water permeances in PV and RO was made by using generalized SD equations.

Theory

Conventional solution-diffusion model

The solution-diffusion model is widely accepted for the explanation of transport behavior in RO, PV, and gas permeation.[29,30] The schema of permeation in a solution-diffusion film are schematically presented with symbols in Figure 1

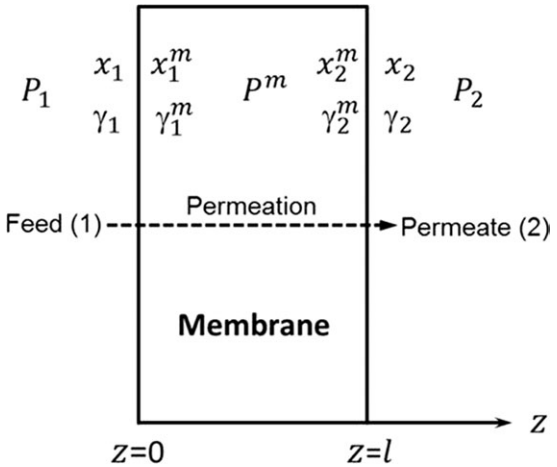

Figure 1. Schematic illustration of permeation through a solution-diffusion membrane.

In the case of RO, the volume flux of water J_v, is expressed as follows

$$J_v = L_p(\Delta P - \Delta\pi), \tag{1}$$

where L_p is the water permeability and, ΔP ($= P_1 - P_2$) and $\Delta\pi$ ($= \pi_1 - \pi_2$) are the differences in applied pressure and osmotic pressure, respectively. The osmotic pressure π, is given by

$$\pi = \phi C_s RT \tag{2}$$

where ϕ is the osmotic coefficient, C_s is the molar concentration of ions, R is the gas constant, and T is the absolute temperature. For dilute solutions, ϕ is reasonably assumed to be unity for the Van't Hoff equation. Similarly, according to the SD model, a simplified expression for salt flux J_s, is given by

$$J_s = B(C_f - C_p) \tag{3}$$

where B is the salt permeability, and C_f and C_p are the salt concentrations in the feed and permeate, respectively.

Flux in PV can be expressed with permeance in PV, P_{PV}, and vapor pressure difference across a membrane ($P_{sat} - P_2$), since the driving force of the permeating molecules is the vapor pressure $P_{sat} = P_1$. When the vapor pressure in the permeate P_2 is assumed to be zero, permeate flux can be expressed as follows

$$J = P_{PV}(P_{sat} - P_2) = P_{PV} \cdot P_{sat} \tag{4}$$

A similar equation is conventionally applied to gas permeation, using pressure difference between the feed and permeate sides, as follows

$$J = P_{GS}(P_1 - P_2) \tag{5}$$

Generalized solution-diffusion model

The generalized SD model assumes that the diffusion coefficient D, activity coefficient γ^m, and total molar concentration C^m, are constant; the pressure within a membrane P^m, is uniform and equal to upstream pressure P_1; and, the molar

volume of a permeant $\overline{v}$, is constant, and is not dependent on the pressure. According to the SD model, permeating molar flux is obtained as the product of diffusivity and concentration difference in the membrane and formulated for RO and PV as follows[30]

$$\text{RO}: \quad J = \frac{DC^m}{\ell}\left(\frac{\gamma_1 x_1}{\gamma^m} - \frac{\gamma_2 x_2}{\gamma^m}\exp\left(\frac{\overline{v}}{RT}(P_2 - P_1)\right)\right) \tag{6}$$

The osmotic pressure, π, is defined, using activity, a ($= \gamma x$), as follows

$$\pi = \frac{RT}{\overline{v}}\ln(a) = \frac{RT}{\overline{v}}\ln(\gamma x) \tag{7}$$

Thus, Eqs. 6 and 7 can be combined to yield

$$\begin{aligned} J &= \frac{DC^m}{\ell}\left(\frac{\gamma_1 x_1}{\gamma^m} - \frac{\gamma_1 x_1}{\gamma^m}\exp\left(\frac{\overline{v}}{RT}(\pi_1 - \pi_2)\right)\right. \\ &\quad \left.\times \exp\left(\frac{\overline{v}}{RT}(P_2 - P_1)\right)\right) \\ &= \frac{DC^m}{\gamma^m \ell}\gamma_1 x_1\left(1 - \exp\left(\frac{\overline{v}}{RT}(\Delta P - \Delta\pi)\right)\right) \end{aligned} \tag{8}$$

Under the RO test conditions ΔP ($= P_1 - P_2$) $= 1.15 \times 10^6$ Pa, $\Delta\pi$ ($= \pi_1 - \pi_2$) $\approx 0.17 \times 10^6$ Pa, $T = 298$–363 K, and $\overline{v} = 18 \times 10^{-6}$ m^3/mol; the term $\overline{v}(\Delta P - \Delta\pi)/RT$ is from 5.8×10^{-3} to 7.1×10^{-3}. Since this term is very small, the simplification $1 - \exp(x) \to x$ as $x \to 0$ can be applied, and a very good approximation of Eq. 8 can be written as follows

$$J = \frac{DC^m}{\gamma^m \ell}\gamma_1 x_1 \frac{\overline{v}}{RT}(\Delta P - \Delta\pi) \tag{9}$$

$$\text{PV}: \quad J = \frac{DC^m}{\ell}\left(\frac{\gamma_1 x_1}{\gamma^m} - \frac{P_2 x_2}{\gamma^m P_{\text{sat}}}\exp\left(\frac{\overline{v}}{RT}(P_{\text{sat}} - P_1)\right)\right) \tag{10}$$

Under the PV test conditions, $\overline{v} = 18 \times 10^{-6}$ m^3/mol, $P_1 = 10^5$ Pa, $T = 363$ K, $P_{\text{sat}} \approx 0.7 \times 10^5$ Pa; the term $\exp(\overline{v}(P_{\text{sat}} - P_1)/RT) \approx 1$. Equation 10 can be written as

$$J = \frac{DC^m}{\ell}\left(\frac{\gamma_1 x_1}{\gamma^m} - \frac{P_2 x_2}{\gamma^m P_{\text{sat}}}\right) = \frac{DC^m}{\gamma^m \ell}\left(\gamma_1 x_1 - \frac{P_2 x_2}{P_{\text{sat}}}\right) \tag{11}$$

Therefore, the permeance in PV combining Eqs. 4 and 11, can be expressed as follows

$$P_{PV} = \frac{DC^m \gamma_1 x_1}{\gamma^m \ell}\frac{1}{P_{\text{sat}}} \tag{12}$$

While the permeance in RO, P_{RO}, is defined on a molar basis, a comparison of Eqs. 1 and 9 is, as follows

$$P_{\text{RO}} = \frac{L_p}{\overline{v}} = \frac{DC^m \gamma_1 x_1}{\gamma^m \ell}\frac{\overline{v}}{RT} \tag{13}$$

Equations 12 and 13 give the conversion relationship between conventional and generalized SD model, and a quantitative comparison of permeance in RO and PV.

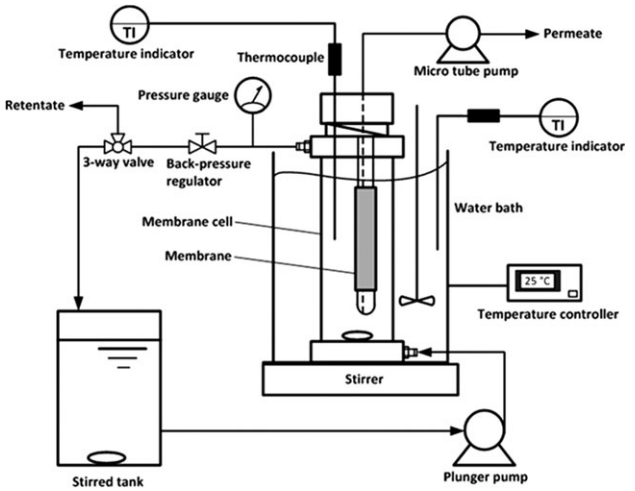

Figure 2. Schematic diagram of the reverse osmosis experiment.

Experimental

Synthesis of BTESE-derived organosilica sol

BTESE polymer sols were synthesized by the hydrolysis and polymerization reaction of BTESE (Gelest, Inc.) in ethanol. The detailed procedure has been described elsewhere.[28] Briefly, BTESE was mixed at the molar ratio of BTESE/H_2O/HCl = 1/60/0.1 with the equivalent weight of BTESE kept at 5.0 wt %. After stirring for 2 h at room temperature, the BTESE polymer sols were used to prepare the separation layer of the organosilica membranes.

Membrane fabrication and characterization

Tubular α-alumina microfiltration membranes (porosity, 50%; average pore size, 1 μm; outside diameter, 10 mm; length, 100 mm) were used as the supports. First, α-alumina powders (average particle size: 0.2, 1.9 μm) were coated onto the outer surface of the support using silica-zirconia colloidal sols as a binder, and the support was fired at 550°C for 30 min. This coating and firing process was repeated several times to remove large pores that might have caused pinholes in the membrane. Then, SiO_2-ZrO_2 colloidal sols (molar ratio of Si/Zr = 1/1) were coated onto the substrate and fired at 550°C to form an intermediate layer. Finally, the BTESE polymer sol was deposited onto the intermediate layer, followed by calcination in nitrogen at 100 or 300°C for 30 min. After preparation, the membrane morphology and thickness were examined using a scanning electron microscope (SEM) (JCM-5700, JEOL) with an acceleration voltage of 20 kV.

Reverse osmosis, gas permeation, and pervaporation measurements

Figure 2 shows the schematic diagram of the RO experimental apparatus. The membrane was installed vertically inside a RO cell. The feed solution, pressurized with a plunger pump in the range of 0.5–1.5 MPa, was vigorously agitated using a magnetic stirrer at 800 rpm in the cell, and the retentate was recycled back to the feed container at an approximate flow of 30 mL/min. The permeate stream was maintained at atmospheric pressure, and collected using a micro tube pump. The temperature of the feed solution was controlled at 25–90°C using a water bath. The concentrations of solute in the feed (C_f), and permeate (C_p), were measured with a conductivity meter (HORIBA, ES-51) for electrolytes

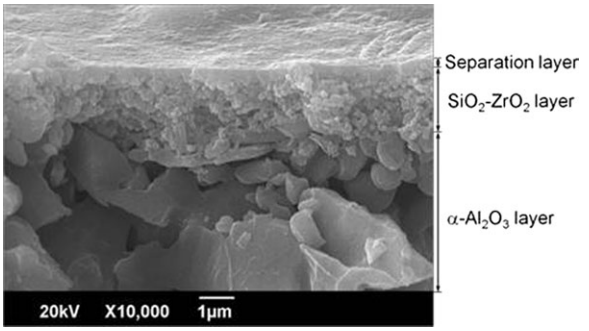

Figure 3. Cross-sectional SEM image of the BTESE-derived organosilica membrane.

and a total organic carbon analyzer (Shimadzu, TOC—V_E) for neutral solutes. The observed rejection R_{obs}, is expressed as follows

$$R_{obs} = \left(1 - C_p/C_f\right) \times 100\% \quad (14)$$

The effect of concentration polarization was rationally ignored in this study due to the low permeate flux. Each RO test lasted for at least 3 h to confirm a steady water flux and rejection, and then the permeate sample was collected at a predetermined time interval. Each experimental data point reported in this article is the average value of 3 samples. The variation in water permeability and observed rejection during each measurement was found to be less than 3.6% and 0.7%, respectively.

Gas permeation measurements were performed at 200°C using a high-purity single component of He, H_2, CO_2, N_2, CH_4, C_3H_8 and SF_6. Before the measurement, the membrane was first pretreated for 8–10 h in a He flow of 50 mL/min at 200°C to remove the adsorbed water from the membrane pores. The permeate side was kept at atmospheric pressure, and the pressure drop through the membrane was maintained at 1 bar. The permeation rate was measured using a soap-film flow meter.

The PV experiments were carried out using a typical PV testing apparatus as previously reported.[34] The membrane was dipped into a 2,000 ppm NaCl solution, which was circulated vigorously to minimize the effect of concentration polarization on the membrane surface. The pressure on the feed side was maintained at atmospheric pressure, whereas the permeate side was evacuated to less than 300 Pa using a vacuum pump. Permeate was collected in liquid nitrogen cold traps during a predetermined time interval.

Results and Discussion

Membrane morphology and reverse osmosis performance

A hybrid organosilica layer was prepared by coating BTESE polymer sol onto the silica-zirconia intermediate layer, followed by drying and calcination at either 100 or 300°C. Figure 3 presents the SEM image of a cross section of a BTESE-derived organosilica membrane. As shown in this micrograph, a crack-free, continuous separation layer formed on the top of the SiO_2-ZrO_2 intermediate layer, and the thin separation layer had a thickness of approximate 200 nm.

The observed rejection and water permeability of the membranes were measured at 25°C and 1.15 MPa, using a series of electrolytes and neutral solutes of different sizes: NaCl (hydrated size of $Na^+_{(aq)}$: 0.72 nm, and $Cl^-_{(aq)}$: 0.66 nm); $MgSO_4$ ($Mg^{2+}_{(aq)}$: 0.86 nm, and $SO^{2-}_{4\,(aq)}$: 0.76 nm);[35] ethanol (Stokes dia. 0.4 nm); isopropyl alcohol (IPA, 0.48 nm); and, glucose (0.73 nm).[36] Figure 4 shows the RO performance of a BTESE-derived organosilica membrane for these probe molecules of different sizes. At a pressure of 1.15 MPa, the membrane calcined at 300°C (BTESE-300) almost completely rejected electrolytes (>98%) and neutral solutes of low-molecular-weight (IPA, 96.9%; glucose, 98.3%), approximately the same level of rejections as seawater desalination membranes. The incomplete rejection of glucose might be due to the pore-size distribution of amorphous silica networks. The preparation procedure will be further optimized to obtain a sharp pore size distribution. However, ethanol afforded only moderate rejection (≈76.0%), because the Stokes diameter of ethanol is smaller than other neutral molecules (IPA, glucose). Its superior capacity for rejection of salts and small organic molecules demonstrated that the BTESE membrane showed great promise as a RO membrane. In addition, the neutral solutes with a larger Stokes diameter showed a higher rejection in the RO process. Since the Donnan effect was ineffective on these neutral solutes, this observation led us to the tentative conclusion that the transport mechanism for the BTESE membrane was primarily based on the molecular sieving effect. This assumption will be further discussed in the following sections.

Effects of operating pressure and feed concentration

Figure 5 shows the effect of feed pressure on permeation of water and salt, using 2 organosilica membranes with different calcination temperatures. Both the water flux (J_v) and the salt rejection (R_{obs}) of BTESE-100 and BTESE-300 membranes increased continuously as operating pressure increased from 0.7 to 1.5 MPa (Figure 5a). The water permeability (L_p), and salt permeability (B) of the two membranes, obtained by Eqs. 1 and 3, were almost constant (Figure 5b). This can be explained by the conventional SD model described by the simplified Eqs. 1–3. The transmembrane pressure difference ($\Delta P - \Delta\pi$) is the driving force for water transport across the membrane. Therefore, the water flux increased linearly with increasing the operating pressure, and the water permeability remained almost constant

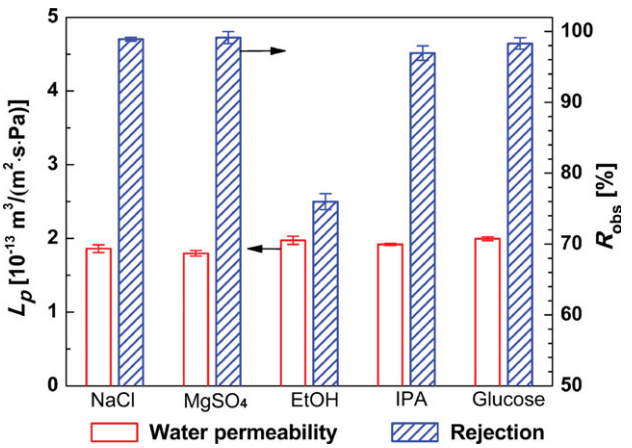

Figure 4. Rejection and water permeability of the BTESE-300 membrane for 5 types of probe molecules at a temperature of 25°C and a pressure of 1.15 MPa.

[Color figure can be viewed in the online issue, which is available at wileyonlinelibrary.com.]

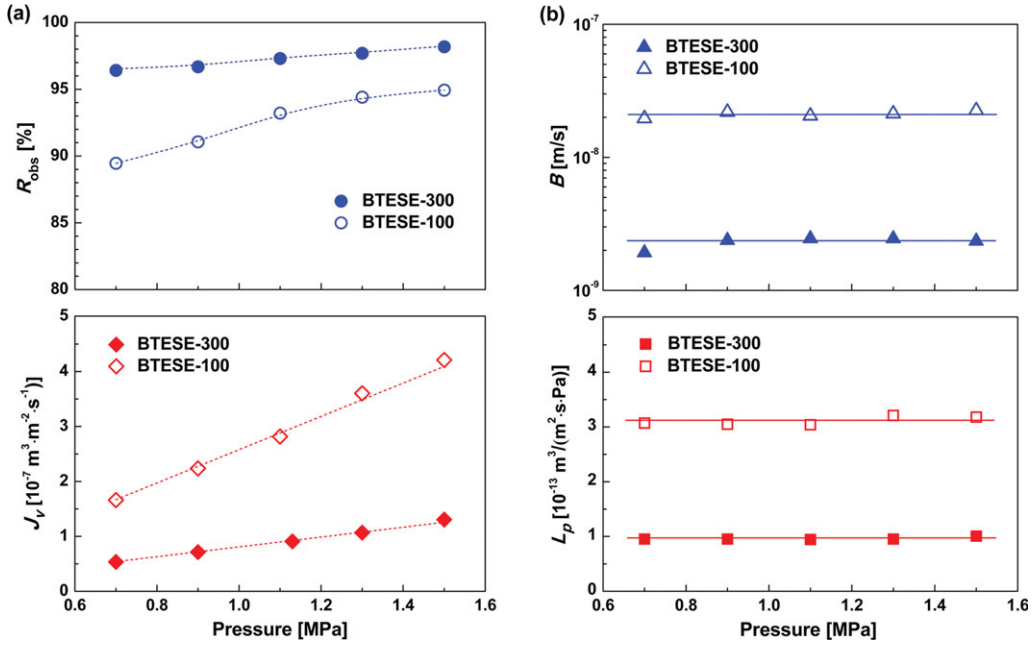

Figure 5. Effect of operating pressure on water flux and salt rejection (a), and on water permeability and salt permeability (b) at 25°C and 2,000-ppm NaCl feed (Dotted curves are calculated using Eqs. 1, 2, 3, and 15 with membrane parameters L_p and B).

[Color figure can be viewed in the online issue, which is available at wileyonlinelibrary.com.]

throughout the operating pressure range. However, the driving force for ion permeation through the membrane, according to Eq. 3, is the transmembrane concentration gradient. In other words, the salt flux (J_s) is independent of the operating pressure. Therefore, the salt permeability (B) was nearly constant, as shown in Figure 5b. Eventually, the salt rejection increased gradually with feed pressure due to the enhanced water permeation (Figure 5a). Using the relationships of water and salt permeability, the theoretical salt rejection of the SD model can be expressed as follows[37]

$$R = \frac{L_p(\Delta P - \Delta\pi)}{L_p(\Delta P - \Delta\pi) + B} \times 100\% \tag{15}$$

Equation 15 relates salt rejection to intrinsic transport properties of the membrane (L_p and B), and the operating conditions (ΔP and $\Delta\pi$). The dotted curves in Figure 5a were calculated using averages for L_p and B, as shown in Figure 5b, and showed excellent agreement with experimentally obtained flux J_v, and rejection R_{obs}.

It should be noted that the BTESE-300 membrane exhibited higher rejection and lower water flux than the BTESE-100 membrane. This difference in the separation performance can be attributed to effective pore-size variation of the organosilica network that occurred in the calcination process. Calcination at higher temperatures accelerated the condensation reaction of silanol groups (dehydroxylation) on the network and the formation of siloxane bonds, thus, resulting in a denser silica network structure.[22,38]

The desalination performance of the BTESE-300 membrane was evaluated using NaCl concentrations varied from 500 to 10,000 ppm. The filtration performances of these NaCl solutions at a constant pressure of 1.5 MPa are illustrated in Figure 6. Increasing the feed concentration led to a decrease in transmembrane pressure difference ($\Delta P - \Delta\pi$)

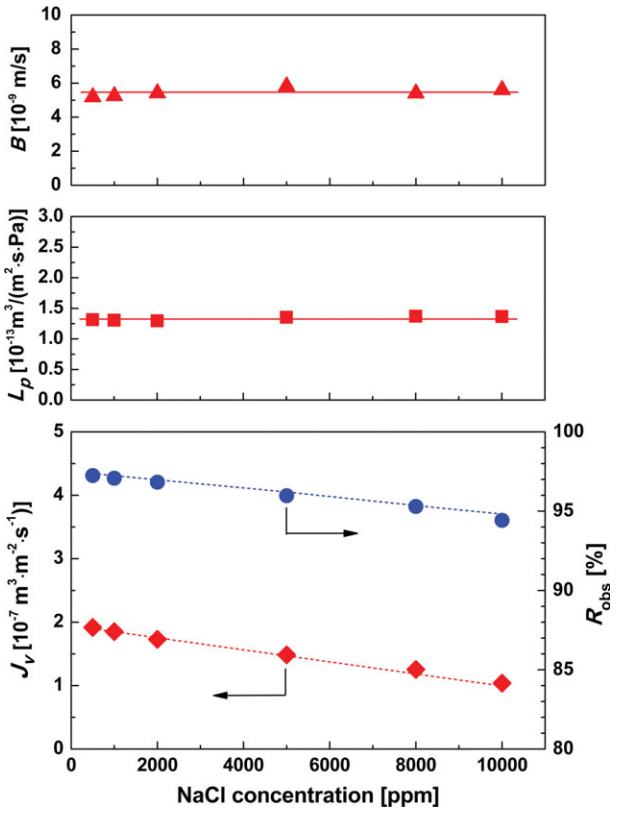

Figure 6. Influence of NaCl concentration on the permeation performance of the BTESE-300 membrane at 25°C and 1.5 MPa (Dotted curves are calculated using Eqs. 1–3, and Eq. 15 with membrane parameters L_p and B).

[Color figure can be viewed in the online issue, which is available at wileyonlinelibrary.com.]

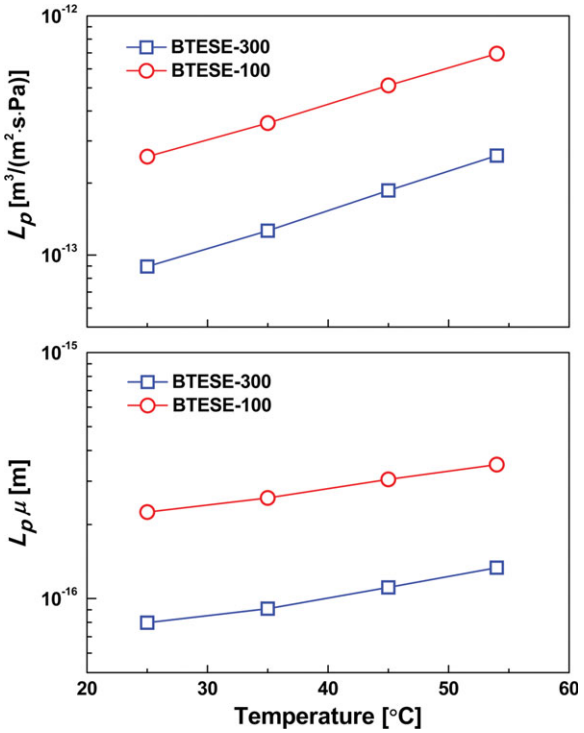

Figure 7. Temperature dependence of water permeability L_p, and viscosity-corrected water permeability, $L_p\mu$, for BTESE-300 and BTESE-100 membranes.

[Color figure can be viewed in the online issue, which is available at wileyonlinelibrary.com.]

because of the increased osmotic pressure (π) at high ion concentrations (at 25°C, $\pi = 0.04$ MPa, and $\pi = 0.85$ MPa, respectively, for 500-ppm and 10,000-ppm NaCl solution). Consequently, at a constant operating pressure, the water flux fell linearly from 1.9×10^{-7} to 1.0×10^{-7} m^3/(m^2·s) in the concentration range, while the water permeability was nearly constant at approximately 1.3×10^{-13} m^3/(m^2·s&Pa). Since the concentration gradient across the membrane is the driving force for ion permeation, salt flux increased linearly with feed concentration, and salt permeability at any concentration, remained relatively constant. Ultimately, as shown in Figure 6, the salt rejection decreased slightly as the concentration increased, which is in agreement with Eq. 15. Meanwhile, the salt permeability clearly did not show obvious changes. As is well-known, the rejection behavior of the solutes in NF and RO is governed by the charge (Donnan) effect and/or steric (sieving) effect. If the charge effect plays a major role, an increase in the ion concentrations should result in a significant drop in salt rejection, which is often observed for many nanofiltration membranes.[39] Therefore, the observation that the salt permeability remained approximately constant indicates that the influence of charge-charge interactions between the ions and micropores of silica networks has only a minor effect on the transport of ions through the membrane. This provides additional evidence that the transport mechanism for the BTESE RO membranes is governed by the molecular sieving effect.

Temperature dependence of RO performance

The water permeation performance of the membrane as a function of temperature is shown in Figure 7. As temperature increased from 25 to 55°C, the water permeability of two BTESE membranes with different calcination temperatures increased two- to three-fold. According to the viscous flow mechanism, the permeability through porous membranes (effective pore size r_p; effective membrane thickness, Δx; and porosity A_k) is formulated as the following Hagen-Poiseuille equation:[40]

$$L_p\mu = r_p^2 A_k / 8\Delta x \tag{16}$$

If the transport mechanism through these micropores is the viscous flow mechanism, the viscosity-corrected water permeability $L_p\mu$, defined as L_p multiplied by the viscosity of bulk water (μ), should be constant regardless of the permeation temperature, since the structural parameters on the right side of Eq. 16 are considered to be constant. As shown in Figure 7, the $L_p\mu$ of the two kinds of BTESE membranes was not constant and clearly increased with temperature. Our group and others have observed a similar temperature dependency for inorganic NF membranes in water and many different organic solvents systems.[40–42] Figure 8 shows $L_p\mu$ normalized with that at 25°C for the BTESE RO membranes in a comparison with the previous SiO_2-ZrO_2 and TiO_2 NF membranes. The normalized $L_p\mu$ should be unity if the water permeation obeys the viscous flow mechanism. However, it is obvious that the normalized $L_p\mu$ increased as temperature increased, and the slope increased on the order of BTESE-300>BTESE-100>SiO_2-ZrO_2>TiO_2, which is in accordance with the order of MWCO values (Table 1). The membrane with smaller pores showed a larger deviation from the viscous flow behavior. The dependency on permeation temperature can be evaluated by the Arrhenius equation with the activation energy of permeability. Table 1 summarizes the observed activation energies of L_p and $L_p\mu$ for BTESE, SiO_2-ZrO_2 and TiO_2 membranes. Clearly, the membrane with the smaller pore size showed larger activation energy. Meanwhile, the observed activation energies were larger than the corresponding viscosity activation energy, which again suggests that the water permeation through BTESE-derived organosilica membranes was different from viscous flow.

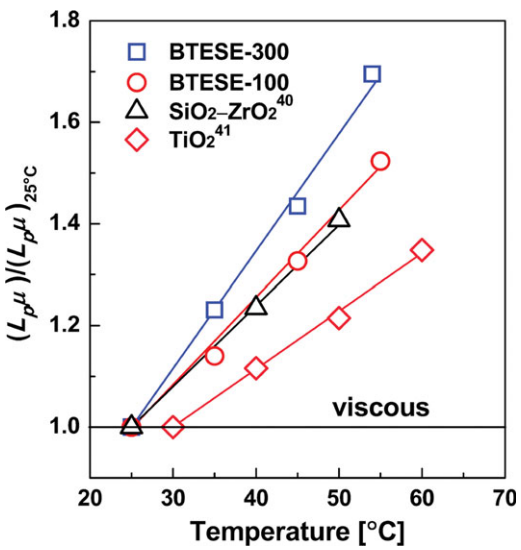

Figure 8. Normalized $L_p\mu$ as a function of temperature.

[Color figure can be viewed in the online issue, which is available at wileyonlinelibrary.com.]

Table 1. Activation Energy of L_p and $L_p\mu$ for BTESE RO Membranes, Compared with Silica-Zirconia and Titania NF Membranes

Membrane	BTESE-300 (MWCO[c]: 50)[33]	BTESE-100 (MWCO: 100)[33]	SiO_2-ZrO_2[40] (MWCO: 200)	TiO_2[41] (MWCO: 600)	viscous flow[b]
$\Delta E(L_p)$ (kJ/mol)[a]	30.8	27.1	24.6	22.7	15.4
$\Delta E(L_p\mu)$ (kJ/mol)[a]	15.3	12.1	/	8.2	0

[a]Activation energies $\Delta E(L_p)$ and $\Delta E(L_p\mu)$ were obtained using $L_p = (L_p)_0 \exp(-\Delta E(L_p)/RT)$, and $L_p\mu = (L_p\mu)_0 \exp(-\Delta E(L_p\mu)/RT)$.
[b]Activation energy of viscous flow was calculated from the temperature dependence of the water viscosity, μ, in the bulk assuming a constant $L_p\mu$.
[c]Molecular weight cutoff (MWCO, g/mol) is defined as the molecular weight at which 90% of a non-charged solute will be retained by the membrane

There are several possible reasons for these phenomena. The first is that water permeation is an activated process in which water molecules permeate through the micropores via a repulsive force from the pore walls. Since the average pore size of the BTESE membrane is estimated to be approximately 0.5 nm,[28] water molecules are expected to have strong friction with the pore walls. As the temperature increases, a portion of water molecules that have sufficient thermal energy to jump the energy barrier can pass through the micropores. Another explanation might be based on adsorption of water on the pore wall. Water can adsorb to hydrophilic parts of the organosilica pore wall that are covered with small amounts of silanol groups. The thickness of adsorbed water decreases with temperature, resulting in larger effective pores for water permeation. Third, the viscosity of water in micropores is different from that in a bulk solution.[40] Therefore, the temperature dependence of viscosity in these pores might be higher than that of the bulk solution.

To further investigate the influence of temperature on desalination performance, the water permeability and NaCl rejection of the BTESE-300 membrane were measured in temperature cycle experiments. As presented in Figure 9, the feed temperature was increased and decreased step by step. After each step reached a steady state (ca. 3 h), the membrane performance was then measured. With an increase in temperature from 25 to 90°C, the water permeability increased approximately eight-fold. Surprisingly, a tradeoff between water permeability and water/salt selectivity was not observed during this process. On the contrary, NaCl rejection increased slightly as temperature increased and reached 98.3% at 90°C, from an initial value of 97.3% at 25°C. This contrasts with polymeric desalination membranes, for which increased water permeability generally comes at the expense of salt rejection due to thermal expansion of the polymer at high temperature.[37] For example, with the well-known commercial polyamide membrane, NF90, rejection of KCl decreased from 96.6 to 93.2% and water permeability increased from 3.5 to 11.5 kg/(m^2·h·bar) as the feed temperature increased from 20 to 60°C (at 0.6 MPa, pH 6, and 20 mM KCl).[43] However, thermal expansion effects were assumed to be less pronounced for these silica-based hybrid membranes, and therefore the pore size appeared to be unchanged in this temperature range. Increasing the temperature resulted in increased water permeability probably due to decreased viscosity and activated diffusion, whereas the large hydrated ions were still severely hindered due to the small pore sizes of BTESE silica networks. When the feed temperature was decreased gradually back to the starting level, water permeability returned to approximately the initial value, and high salt rejection was maintained. Only a few polymeric NF membranes withstood a temperature cycle of up to 65°C without a significant change in filtration performance.[10,11] The high reproducibility of the RO performance in temperature cycles indicated superior hydrothermal stability of the BTESE membranes, which would benefit applications of high-temperature reverse osmosis.

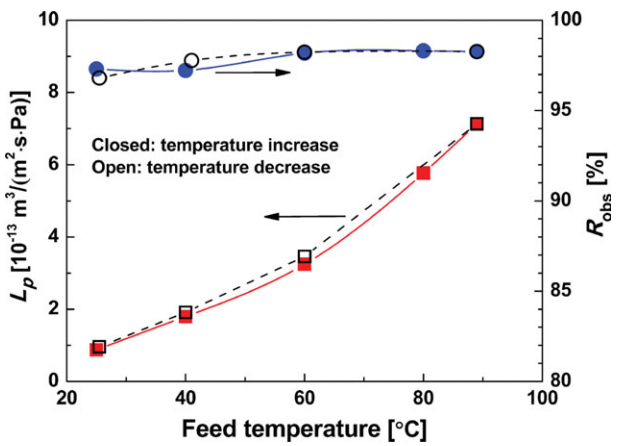

Figure 9. Water permeability and salt rejection for the BTESE-300 membrane as a function of temperature cycles at 1.15 MPa and 2,000-ppm NaCl feed.

[Color figure can be viewed in the online issue, which is available at wileyonlinelibrary.com.]

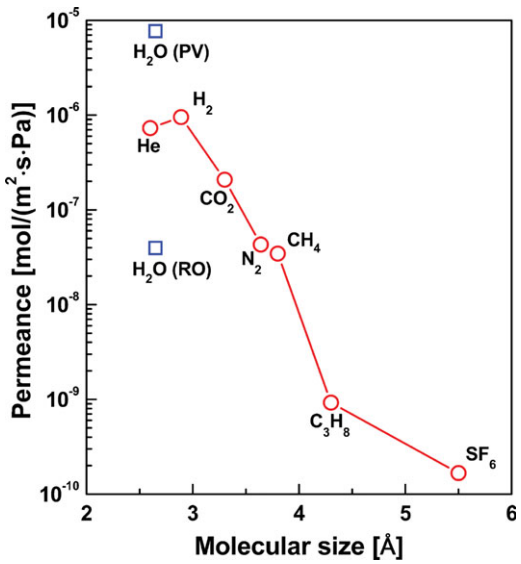

Figure 10. Gas permeance of the BTESE-300 membrane as a function of kinetic diameter at 200°C compared with water permeance in PV and RO processes at 90°C.

[Color figure can be viewed in the online issue, which is available at wileyonlinelibrary.com.]

Table 2. Comparison of Desalination Performance of BTESE Membranes and some Typical RO Membranes

Membrane	Testing conditions	Flux [L/(m^2·h)]	Water permeability [m^3/(m^2·s·Pa)]	Rejection [%]	Ref.
ZSM-5, Si/Al = 50	25°C, 2.76 MPa, 0.1M-NaCl	1.129	1.4×10^{-13}	92.9	[13]
Silicalite	25°C, 2.76 MPa, 0.1M-NaCl	0.112	1.4×10^{-14}	90.6	[13]
Silicalite	25°C, 2.76 MPa, 0.1M-NaCl	0.35	4.3×10^{-14}	99.4	[14]
SW30HR (FilmTec)[a]	21°C, 2.76 MPa, 2000 ppm-NaCl	21 ± 5	$(2.2 \pm 0.5) \times 10^{-12}$	98.5 ± 0.7	[7]
ES10 (Nitto Denko)[b]	24°C, 1.0 MPa, 104 ppm-NaCl	/	$(1.2 \pm 0.16) \times 10^{-11}$	99.2	[49]
BTESE-100	25°C, 1.15 MPa, 2000 ppm-NaCl	/	$(2.8-3.2) \times 10^{-13}$	93.8–94.4	This work
BTESE-300	25°C, 1.15 MPa, 2000 ppm-NaCl	/	$(0.9-1.8) \times 10^{-13}$	97.1–99.2	This work

[a]Membrane type: aromatic polyamide; free chlorine tolerance: <0.1 ppm.[50]
[b]Membrane type: aromatic polyamide; residual chlorine: zero.[50]

Comparison of transport properties and desalination performances

Figure 10 shows water permeances in PV and RO desalination processes with the BTESE-300 membrane, and compares them with gas permeances to develop deeper insight into the properties of water transport through the organosilica membrane. The single gas permeance results revealed that the membrane had hydrogen permeance as high as 1×10^{-6} mol m^{-2} s^{-1} Pa^{-1} with a high H_2/SF_6 permeance ratio of 5700. Water permeance in the PV was nearly one order of magnitude higher than the permeance of gases with similar kinetic diameters, such as He and H_2. This can probably be attributed to an increment in the adsorptive property of the water molecules. Water molecules that adsorbed to the hydrophilic parts of the organosilica networks could easily diffuse through the membrane by surface diffusion mechanism, avoiding strong interactions between water molecules and membrane pore walls. Similar observations have been reported in zeolite-4A membranes[44] and carbon membranes.[45] It is noteworthy that the transmembrane pressure difference was approximately 1 MPa in RO, resulting in a water flux of 2.4 kg/(m^2·h), whereas the vapor pressure difference was approximately 70 kPa in PV at 90°C, giving a flux of 34.9 kg/(m^2·h). For comparison, L_p [m^3/(m^2·s·Pa)] was converted to P_{RO} ($P_{RO} = L_p/v_w$) in mol/(m^2·s·Pa), and very low water permeance was obtained in RO.

The difference in water permeance, as shown in Figure 10, can be explained by application of the generalized SD equations for RO and PV processes. Within the context of the generalized SD model, by comparing Eqs. 12 and 13 the permeance difference in PV and RO is found in the terms $1/P_{sat}$ and $\overline{v}/RT$. The generalized transport equations suggest that the PV and RO are directly connected, and the permeation performance in one mode can be used to provide an initial estimate of performance in the other mode. For example, one can calculate theoretical PV desalination performance using the RO desalination performance data. In this study, the theoretical ratio of water permeance in RO to that in PV was calculated to be approximately 0.04% at 90°C, and the experimentally obtained ratio was 0.5% at this temperature. The generalized SD model successfully explained the drastic decrease in RO permeance, compared with that of PV. This is because a larger chemical potential difference could be provided for PV due to very low permeate pressure. Quantitatively, the water permeance in PV was predicted to be overstated, since the prediction of PV performance was made under ideal conditions. First, the PV process is theoretically considered as isothermal in the radial direction to the membrane. In reality, however, there is usually a noticeable temperature decrease from the bulk liquid to the upstream membrane surface.[46] This temperature drop in the liquid boundary layer could lead to a significant drop in water permeance due to the decrease in water vapor pressure, and, therefore, the driving force. Second, the nanoporous intermediate layer of this membrane is suspected to offer extra resistance to the transport of water molecules, particularly in PV with high flux, thus, inhibiting the observation of expected high water permeance in PV.[47] Third, in the PV desalination experiment, small amounts of hydrated Na and Cl ions may have diffused through to the permeate side and built-up on the surface of the permeate side, since they cannot evaporate under a vacuum.[48] The accumulation of ions on the permeate surface would increase with experimental time, and decrease the water permeance.

Table 2 summarizes the desalination performance in RO of BTESE-derived organosilica membranes, typical zeolite membranes, and commercial polyamide membranes. Compared with inorganic zeolite membranes such as ZSM-5 and silicalite, BTESE membranes showed higher water permeability. While the commercial polyamide RO membranes (seawater RO membrane, SW30HR; low-pressure RO membrane, ES10) had higher water permeability than BTESE membranes, these polyamide membranes suffered from poor resistance to chlorine, the concentration of which was normally recommended to be lower than 0.1 ppm.[50] BTESE membranes had already exhibited high chlorine tolerance over a wide range of chlorine concentration (from 100 to 1,000 ppm active chlorine) in our previous study, showing great promise as a new type of chlorine-resistant RO membrane materials.[33] Further studies are being focused on optimizing the surface chemistry and network structure of the membrane to improve the water permeability and salt rejection while maintaining its high robustness.

Conclusions

Hybrid organosilica membranes were prepared by a sol–gel technique using bis(triethoxysilyl)ethane (BTESE), and were applied to desalination by reverse osmosis (RO). The influences of solute species, calcination temperatures, operating pressure, feed concentration and feed temperature were systematically studied to determine the permeation performance and transport mechanism of this new type of RO membrane. The generalized solution-diffusion (SD) equations were applied for a quantitative comparison of water permeance in PV and RO desalination processes using the same organosilica membrane.

1. BTESE-derived organosilica membrane showed superior retention performance for mono- and bivalent ions and neutral solutes of low-molecular-weight, such as isopropyl alcohol and glucose. The membrane calcined at 300°C exhibited higher salt rejection and lower water flux compared with the membrane prepared at 100°C, due to the

formation of a denser silica network structure in the calcination process.

2. As the operating pressure increased from 0.7 to 1.5 MPa, both the water flux and the salt rejection increased continuously, and the water permeability and salt permeability were almost constant. The pressure dependence of the permeation performance was explained well by the conventional SD model. The theoretical salt rejection and water flux showed excellent agreement with the experimental values.

3. The water flux decreased linearly as the salt concentration increased from 500 to 10,000 ppm, and the salt rejection decreased slightly with salt concentration. The nearly constant salt permeability in the concentration range excluded governance of the transport mechanism by the charge effect, thus, supporting the molecular sieving mechanism for the organosilica RO membranes.

4. The water permeation mechanism was found to differ from the viscous flow mechanism. Observed activation energies of permeation increased with a smaller pore size (lower MWCO values) for RO and NF membranes, and were considerably larger than the activation energies of the solvent viscosity. The organosilica membranes showed exceptional hydrothermal stability in temperature cycles in comparison with commercial polyamide RO membranes. The water permeability increased approximately eight-fold and salt rejection also increased slightly with an increase in temperature up to 90°C.

5. The applicability of the generalized SD model was examined in RO and PV desalination processes. The generalized transport equations were useful in providing a quick prediction for permeation performance based on performance observed in one mode. The water permeance differences in RO and PV processes agreed with the predictions made by using the generalized SD equations.

Acknowledgments

This research is supported in part by Core Research for Evolutional Science and Technology (CREST) Program of Japan Science and Technology Agency (JST).

Notation

a = activity, dimensionless
A_k = surface porosity, dimensionless
B = salt permeability, $m \cdot s^{-1}$
C = concentration, $mol \cdot m^{-3}$
D = diffusivity, $m^2 \cdot s^{-1}$
J = permeation flux, $m^3 \cdot m^{-2} \cdot s^{-1}$
L_p = water permeability, $m^3 \cdot m^{-2} \cdot s^{-1} \cdot Pa^{-1}$
P = pressure, Pa
P_{sat} = saturation vapor pressure, Pa
P_{PV}, P_{RO}, and P_{GS} = permeance in pervaporation, reverse osmosis, and gas separation, $mol \cdot m^{-2} \cdot s^{-1} \cdot Pa^{-1}$
R = gas constant, $J \cdot mol^{-1} \cdot K^{-1}$
R_{obs} = observed rejection, dimensionless
R = theoretical salt rejection, dimensionless
r_p = pore radius, m
T = temperature, K
x = mole fraction, dimensionless
Δx, ℓ = membrane thickness, m

Greek letters

ϕ = osmotic coefficient, dimensionless
γ = activity coefficient, dimensionless
μ = viscosity, Pa·s
$\bar{v}$ = molar volume, $m^3 \cdot mol^{-1}$
π = osmotic pressure, Pa

Superscripts

m = inside the membrane

Subscripts

f, p = feed stream, permeate stream
s = salts
w = water
1, 2 = feed and permeate stream in diffusion

Literature Cited

1. Shannon MA, Bohn PW, Elimelech M, Georgiadis JG, Marinas BJ, Mayes AM. Science and technology for water purification in the coming decades. *Nature*. 2008;452:301–310.
2. Greenlee LF, Lawler DF, Freeman BD, Marrot B, Moulin P. Reverse osmosis desalination: water sources, technology, and today's challenges. *Water Res*. 2009;43:2317–2348.
3. Lee KP, Arnot TC, Mattia D. A review of reverse osmosis membrane materials for desalination-development to date and future potential. *J Membr Sci*. 2011;370:1–22.
4. Mansouri J, Harrison S, Chen V. Strategies for controlling biofouling in membrane filtration systems: challenges and opportunities. *J Mater Chem*. 2010;20:4567–4586.
5. Glater J, Hong SK, Elimelech M. The search for a chlorine-resistant reverse osmosis membrane. *Desalination*. 1994;95:325–345.
6. Zhou MJ, Nemade PR, Lu XY, Zeng XH, Hatakeyama ES, Noble RD, Gin DL. New type of membrane material for water desalination based on a crosslinked bicontinuous cubic lyotropic liquid crystal assembly. *J Am Chem Soc*. 2007;129:9574–9575.
7. Hatakeyama ES, Gabriel CJ, Wiesenauer BR, Lohr JL, Zhou MJ, Noble RD, Gin DL. Water filtration performance of a lyotropic liquid crystal polymer membrane with uniform, sub-1-nm pores. *J Membr Sci*. 2011;366:62–72.
8. Park HB, Freeman BD, Zhang ZB, Sankir M, McGrath JE. Highly chlorine-tolerant polymers for desalination. *Angew Chem Int Ed*. 2008;47:6019–6024.
9. Snow JHM, Winter DD, Buckingham R, Campbell J, Wagner J. New techniques for extreme conditions: high temperature reverse osmosis and nanofiltration. *Desalination*. 1996;105:57–61.
10. Mänttäri M, Pihlajamäki A, Kaipainen E, Nyström M. Effect of temperature and membrane pretreatment by pressure on the filtration properties of nanofiltration membranes. *Desalination*. 2002;145:81–86.
11. Saidani H, Amar NB, Palmeri J, Deratani A. Interplay between the transport of solutes across nanofiltration membranes and the thermal properties of the thin active layer. *Langmuir*. 2010;26:2574–2583.
12. Li LX, Dong JH, Nenoff TM, Lee R. Desalination by reverse osmosis using MFI zeolite membranes. *J Membr Sci*. 2004;243:401–404.
13. Li LX, Liu N, McPherson B, Lee R. Enhanced water permeation of reverse osmosis through MFI-type zeolite membranes with high aluminum contents. *Ind Eng Chem Res*. 2007;46:1584–1589.
14. Liu N, Li LX, McPherson B, Lee R. Removal of organics from produced water by reverse osmosis using MFI-type zeolite membranes. *J Membr Sci*. 2008;325:357–361.
15. Duke MC, O'Brien-Abraham J, Milne N, Zhu B, Lin JYS, da Costa JCD. Seawater desalination performance of MFI type membranes made by secondary growth. *Sep Purif Technol*. 2009;68:343–350.
16. de Vos RM, Verweij H. High-selectivity, high-flux silica membranes for gas separation. *Science*. 1998;279:1710–1711.
17. Yoshioka T, Nakanishi E, Tsuru T, Asaeda M. Experimental study of gas permeation through microporous silica membranes. *AIChE J*. 2001;47:2052–2063.
18. ten Elshof JE, Abadal CR, Sekulić J, Chowdhury SR, Blank DHA. Transport mechanisms of water and organic solvents through microporous silica in the pervaporation of binary liquids. *Micropor Mesopor Mater*. 2003;65:197–208.
19. Duke MC, da Costa JCD, Do DD, Gray PG, Lu GQ. Hydrothermally robust molecular sieve silica for wet gas separation. *Adv Funct Mater*. 2006;16:1215–1220.
20. Igi R, Yoshioka T, Ikuhara YH, Iwamoto Y, Tsuru T. Characterization of Co-doped silica for improved hydrothermal stability and application to hydrogen separation membranes at high temperatures. *J Am Ceram Soc*. 2008;91:2975–2981.
21. Boffa V, Blank DHA, ten Elshof JE. Hydrothermal stability of microporous silica and niobia-silica membranes. *J Membr Sci*. 2008;319:256–263.
22. de Vos RM, Maier WF, Verweij H. Hydrophobic silica membranes for gas separation. *J Membr Sci*. 1999;158:277–288.

23. Campaniello J, Engelen CWR, Haije WG, Pex PPAC, Vente JF. Long-term pervaporation performance of microporous methylated silica membranes. *Chem Commun*. 2004;834–835.
24. Castricum HL, Sah A, Kreiter R, Blank DHA, Vente JF, ten Elshof JE. Hybrid ceramic nanosieves: stabilizing nanopores with organic links. *Chem Commun*. 2008;1103–1105.
25. Castricum HL, Sah A, Kreiter R, Blank DHA, Vente JF, ten Elshof JE. Hydrothermally stable molecular separation membranes from organically linked silica. *J Mater Chem*. 2008;18:2150–2158.
26. van Veen HM, Rietkerk MDA, Shanahan DP, van Tuel MMA, Kreiter R, Castricum HL, ten Elshof JE, Vente JF. Pushing membrane stability boundaries with HybSi® pervaporation membranes. *J Membr Sci*. 2011;380:124–131.
27. Kanezashi M, Yada K, Yoshioka T, Tsuru T. Design of silica networks for development of highly permeable hydrogen separation membranes with hydrothermal stability. *J Am Chem Soc*. 2009;131: 414–415.
28. Kanezashi M, Yada K, Yoshioka T, Tsuru T. Organic-inorganic hybrid silica membranes with controlled silica network size: preparation and gas permeation characteristics. *J Membr Sci*. 2010;348: 310–318.
29. Wijmans JG, Baker RW. The solution-diffusion model: a review. *J Membr Sci*. 1995;107:1–21.
30. Kataoka T, Tsuru T, Nakao S, Kimura S. Permeation equations developed for prediction of membrane performance in pervaporation, vapour permeation and reverse osmosis based on the solution-diffusion model. *J Chem Eng Jpn*. 1991;24:326–333.
31. Kataoka T, Tsuru T, Nakao S, Kimura S. Membrane transport properties of pervaporation and vapor permeation in ethanol-water system using polyacrylonitrile and cellulose acetate membranes. *J Chem Eng Jpn*. 1991;24:334–339.
32. Paul DR. Reformulation of the solution-diffusion theory of reverse osmosis. *J Membr Sci*. 2004;241:371–386.
33. Xu R, Wang JH, Kanezashi M, Yoshioka T, Tsuru T. Development of robust organosilica membranes for reverse osmosis. *Langmuir*. 2011;27:13996–13999.
34. Tsuru T, Sasaki A, Kanezashi M, Yoshioka T. Pervaporation of methanol/dimethyl carbonate using SiO_2 membranes with nano-tuned pore sizes and surface chemistry. *AIChE J*. 2011;57:2079–2089.
35. Firdaous L, Quéméneur F, Schlumpf JP, Maléríat JP. Modification of the ionic composition of salt solutions by electrodialysis. *Desalination*. 2004;167:397–402.
36. Wang XL, Tsuru T, Nakao S, Kimura S. The electrostatic and steric-hindrance model for the transport of charged solutes through nanofiltration membranes. *J Membr Sci*. 1997;135:19–32.
37. Geise GM, Park HB, Sagle AC, Freeman BD, McGrath JE. Water permeability and water/salt selectivity tradeoff in polymers for desalination. *J Membr Sci*. 2011;369:130–138.
38. Zhuravlev LT. The surface chemistry of amorphous silica. Zhuravlev model. *Colloids Surf A Physicochem Eng Asp*. 2000;173:1–38.
39. Peeters JMM, Boom JP, Mulder MHV, Strathmann H. Retention measurements of nanofiltration membranes with electrolyte solutions. *J Membr Sci*. 1998;145:199–209.
40. Tsuru T, Izumi S, Yoshioka T, Asaeda M. Temperature effect on transport performance by inorganic nanofiltration membranes. *AIChE J*. 2000;46:565–574.
41. Tsuru T, Ogawa K, Kanezashi M, Yoshioka T. Permeation characteristics of electrolytes and neutral solutes through titania nanofiltration membranes at high temperatures. *Langmuir*. 2010;26:10897–10905.
42. Dobrak A, Verrecht B, Van den Dungen H, Buekenhoudt A, Vankelecom IFJ, Van der Bruggen B. Solvent flux behavior and rejection characteristics of hydrophilic and hydrophobic mesoporous and microporous TiO_2 and ZrO_2 membranes. *J Membr Sci*. 2010;346:344–352.
43. Nilsson M, Trägårdh G, Östergren K. Influence of temperature and cleaning on aromatic and semi-aromatic polyamide thin-film composite NF and RO membrane. *Sep Purif Technol*. 2008;62:717–726.
44. Zhu W, Gora L, van den Berg AWC, Kapteijn F, Jansen JC, Moulijn JA. Water vapour separation from permanent gases by a zeolite-4A membrane. *J Membr Sci*. 2005;253:57–66.
45. Yoshimune M, Haraya K. Olefin gas dehydration using carbon hollow fiber membranes derived from sulfonated poly(phenyl oxide). *J Jpn Petrol Inst*. 2011;54:119–123.
46. Favre E. Temperature polarization in pervaporation. *Desalination*. 2003;154:129–138.
47. Huang RYM, Feng X. Resistance model approach to asymmetric poly(ether imide) membranes for pervaporation of isopropanol/water mixtures. *J Membr Sci*. 1993;84:15–27.
48. Cho CH, Oh KY, Kim SK, Yeo JG, Sharma P. Pervaporative seawater desalination using NaA zeolite membrane: Mechanisms of high water flux and high salt rejection. *J Membr Sci*. 2011;371:226–238.
49. Kiso Y, Muroshige K, Oguchi T, Hirose M, Ohara T, Shintani T. Pore radius estimation based on organic solute molecular shape and effects of pressure on pore radius for a reverse osmosis membrane. *J Membr Sci*. 2011;369:290–298.
50. Nunes SP, Peinemann KV. *Membrane materials and membrane preparation*. In: Nunes SP, Peinemann KV, eds. *Membrane Technology in the Chemical Industry*. Weinheim: Wiley-VCH; 2001;1–68.

Manuscript received Feb. 8, 2012, revision received May 14, 2012, and final revision received July 10, 2012.